

## MAGNETIC BEARING ACTUATOR DESIGN FOR A GAS EXPANDER GENERATOR

Alexei V. Filatov, Patrick T. McMullen, Lawrence A. Hawkins, and Eric Blumber

CALNETIX, 12880 Moore Street, Cerritos, CA, 90703

afilatov@calnetix.com

### ABSTRACT

A magnetic bearing system for a high-speed cryogenic gas expander generator is presented. The expander represents a new class of such devices that, in contrast to the earlier technologies, makes use of the expanding gas energy by converting it into electrical power. The magnetic bearing and generator constitute a functionally complete unit that can be used in a variety of gas expanders utilizing different expander wheels and operating at various speeds.

In order to obtain a compact design and increase rotor first bending frequency, the axial magnetic bearing is designed to have different pole areas on different sides of the thrust disk. This results in different load capacities in different directions, matching operational conditions of the unit. Regardless this anisotropy, the bearing features linear force vs current dependence.

Radial and angular suspension of the rotor is achieved using two patented homopolar PM-biased radial bearings. The paper discusses design and analysis of these bearings. In spite of the three-dimensional nature of the electromagnetic problem, combination of analytical solution and 2D FEA was found to be an adequate tool for the bearing analysis.

Theoretical predictions of the bearing performance have been found to be in a good agreement with experimental data.

### INTRODUCTION

Gas expanders are used to extract pure gases such as nitrogen, oxygen, and argon from the ambient air utilizing difference in the gas condensation temperatures (cryogenic distillation). During the distillation process, pressurized gas spins an impeller mounted on a shaft connected to some device that produces drug torque, thus limiting the shaft speed and dissipating energy being released during the gas expansion. Conventionally, this energy was dissipated in oil-loading units or atmospheric blowers, and the shaft was supported by oil bearings. The new generation of the gas expanders features permanent magnet direct-drive electrical generator and magnetic bearings. The generator converts the gas energy into electricity supplied into the electrical grid. Using magnetic bearings makes the system completely “oil-free”, thus simplifying its design and eliminating problems associated with using oil in

cryogenic equipment and risks of accidental contamination of the process products.

The design goal was to develop universal generator/bearing module that could be used in a variety of gas expanders utilizing different expander wheels ranging in weight from 0.16 kg (0.35 lb) to 2.3 kg (5.1 lb) and operating at various speeds from 17,800 to 30,000 RPM. Additionally, all configurations needed to operate below the first bending mode of the rotor. This requirement was somewhat difficult because a fairly large thrust rotor was needed to accommodate the axial design load required for the largest expander wheel (up to 1500 lbf towards the impeller). In this paper we describe the magnetic bearing actuator design that allowed us to satisfy all of the above requirements.

### AXIAL MAGNETIC BEARING

One of the components influencing the system rotordynamics the most was the trust disk needed to compensate 1500 lbf (6670 N) of axial loading. While the weight of the disk had essentially a fixed value for the given load, frequency of the first bending mode could be increased by locating this disk as close to the rotor center of mass as possible. In order to achieve this goal, we have developed an anisotropic axial magnetic bearing taking advantage of the fact that higher axial load capacity was required in one direction than in the other: 1500 lbf towards the impeller, while only 500 lbf in the opposite direction. This fact suggested that we could design a magnetic bearing with different pole areas on the opposite sides of the thrust disk and use space available under smaller pole to accommodate one of the mechanical back-up bearings. This arrangement is shown in Figure 1. Since power consumption was not the crucial factor for this system, we found it advantageous to produce bias flux using bias coils rather than permanent magnets.

The force produced by the bearing is

$$F = \frac{1}{2\mu_0} (B_1^2 \cdot A_1 - B_2^2 \cdot A_2), \quad (1)$$

where  $B_1$  and  $B_2$  are the flux densities in the air gaps on the side of the bigger and smaller loadings respectively;  $A_1$  and  $A_2$  are the total pole surface areas, including inner and outer poles, which areas are assumed to be equal.

Without loss of generality, we assign positive

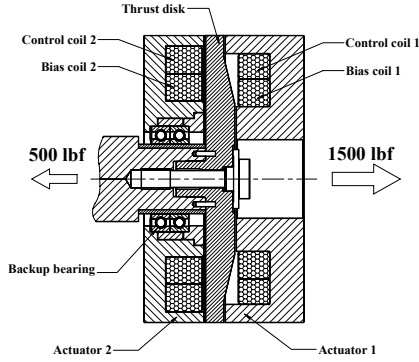


**Figure 1. Asymmetric thrust magnetic bearing.**

signs to both bias fields:  $B_{b1} > 0$  and  $B_{b2} > 0$ .

The total field in each actuator is superposition of the bias and control fields. Again, without loss of generality we assign a positive sign to the control field on the high load side when it is directed as the bias field. Then the equations for the total fields become:

$$B_1 = (B_{b1} + B_{c1}); B_2 = (B_{b2} - B_{c2}); \quad (2)$$

Substituting (2) into (1) yields:

$$F = \frac{1}{2\mu_0} \left( \begin{aligned} & (B_{b1}^2 \cdot A_1 - B_{b2}^2 \cdot A_2) + \\ & (B_{c1}^2 \cdot A_1 - B_{c2}^2 \cdot A_2) + \\ & 2(B_{b1}B_{c1}A_1 + B_{b2}B_{c2}A_2) \end{aligned} \right) \quad (3)$$

The flux densities are assumed to be linear functions of the currents (no saturation occurs):

$$B_{b1} = \mu_0 \frac{N_{b1}I_{b1}}{2g}, \quad B_{b2} = \mu_0 \frac{N_{b2}I_{b2}}{2g},$$

$$B_{c1} = \mu_0 \frac{N_{c1}I_{c1}}{2g}, \quad B_{c2} = \mu_0 \frac{N_{c2}I_{c2}}{2g}, \quad (4)$$

where  $N_{b1}$ ,  $N_{b2}$  are numbers of turns in the bias coils,  $N_{c1}$ ,  $N_{c2}$  are numbers of turns in the control coils, and  $g$  is the air gap between the actuator pole and the thrust disk.

We also assume that

$$I_{b1} = I_{b2} = I_b \text{ and } I_{c1} = I_{c2} = I_c. \quad (5)$$

(coils are connected in series).

It can be observed then from the equation (3), that for the force to be a linear function of the control current, the following condition must be satisfied:

$$B_{c2}^2 A_2 = B_{c1}^2 A_1. \quad (6)$$

Furthermore, for the force to be zero when the control current is zero, we need:

$$B_{b2}^2 A_2 = B_{b1}^2 A_1. \quad (7)$$

Using (4) and (5), equations (6) and (7) can be rewritten as

$$\frac{N_{c1}^2}{N_{c2}^2} = \frac{A_2}{A_1} \text{ and } \frac{N_{b1}^2}{N_{b2}^2} = \frac{A_2}{A_1}. \quad (8)$$

Equations (8) give the desired ratios between the pole surface areas and numbers of turns.

## RADIAL MAGNETIC BEARINGS

While the radial magnetic bearings experience much smaller loads (up to 150 lbf), their design is also extremely important for the overall system performance. In order to minimize the bearing length and maximize the shaft diameter (both result in the increase of the rotor first bending frequency), high magnetic saturation laminations (Carpenter Hipercro 50) were used as a material for the bearing actuator target. This and other measures resulted in a radial bearing actuator design that adds only 1.7 in to the rotor length.

The axial cross-section of the radial bearing is shown in Figure 2. The bearing is a variation of a patented homopolar permanent magnet biased design described in [1]. The bias flux in this bearing is generated by axially magnetized permanent magnets – a solution that results in a more compact and efficient design than when current-carrying coils are used for this purpose. The bias flux flow in the bearing axial plane is illustrated in Figure 3. Currents in the control coils produce magnetic flux in the radial plane of the laminated active pole and the laminated rotor part, which, when superimposed

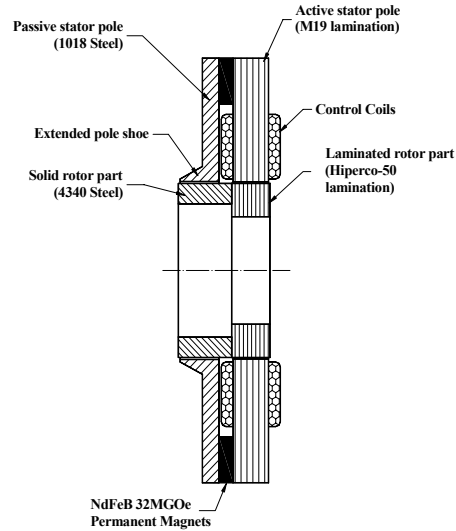


**Figure 2. Axial cross-section of the radial bearing.**

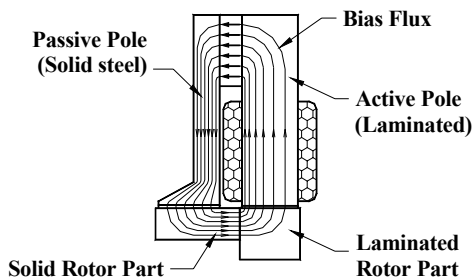


Figure 3. Bias Flux Flow.

on the bias flux, result in radial force proportional to the control current.

Figure 4 clarifies the mechanism of generating radial force. In the upper pole, the control and bias flux sum up, while in the lower pole they subtract. Higher net flux density in the upper air gap results in the radial force acting in the positive Y direction.

A very advantageous feature of this design is that the control flux does not flow through high reluctance permanent magnets. This minimizes size of the control coils as well as their power dissipation.

*Bias flux density calculation*

The electromagnetic analysis of the bias circuit is rather straightforward, and in most part a reasonably

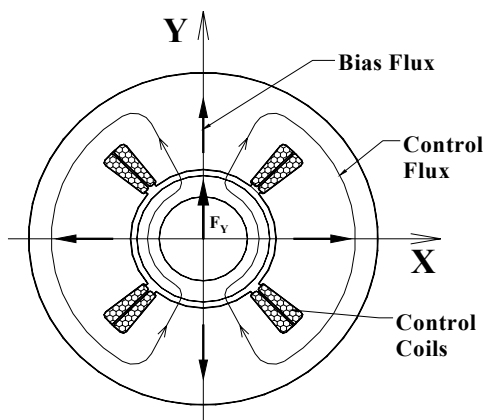


Figure 4. Generation of a radial force.

accurate solution can be obtained analytically. A complication occurs, however, when analyzing bias flux flow in the laminated parts of the system. Since individual laminations are isolated from each other, there exist high-reluctance zones in between the laminations – the circumstance that needs to be taken into account when analyzing flow of the flux entering lamination stack normal to the lamination plane. Two major consequences of this circumstance are a.)

higher reluctance of the magnetic circuit than it would be if the pole were solid, and b.) non-uniform distribution of the magnetic flux density in the control air gap.

If there were no slots accommodating control windings in the active pole, the problem can be attacked using a 2D FEA programs that allows analysis of systems with rotational symmetry. We found particularly convenient using program called FEMM developed by Dr. D. Meeker [2]. In contrast to most commercial FEA packages, FEMM does not require modeling each lamination and insulation in between, but instead models lamination stack as a continuous media with anisotropic magnetic properties.

Winding slots in the control pole, however, eliminate the rotational symmetry and make this problem three dimensional. Nevertheless, we have found it possible to use 2D FEA for solving this problem, if proper adjustments are made to take into account the slot effects.

As the first step, we modify representation of the laminated pole and control gaps in 2D model to make their reluctance match the reluctance of the corresponding 3D counterparts. This allows us to calculate correctly operating tangent of the permanent magnet and magnetic flux density in the rest of the system. Then we calculate magnetic bias flux density in the control air gap, which is of primarily interest to us.

To characterize shape of the winding slots, we introduce pole factor  $K_{pole}$  as a function of the radius  $r$  of a circle with the center on the bearing axis. The pole factor is calculated as ratio of the length of the circle part passing through the iron vs total circle length ( $2\pi r$ ). It is easy to see that when slots are present, magnetic flux crossing the cylinder of radius  $r$  located within the laminated pole and coaxial with the bearing axis is higher than if there were no slots by factor  $1/K_{pole}$ . Higher flux density  $B$  at each point implies higher magnetic strength  $H$ , and higher MMF drop on the laminated pole with slots and control air gap. For the reluctance of laminated pole and control gap in 2D model match the reluctance of their 3D counterparts we need to make the following transformation of the original media  $B(H)$  curve into  $B^*(H^*)$  curve of an equivalent media used in 2D model:

$$H^*(B^*, r) = H(B \cdot 1/K_{pole}(r)). \quad (9)$$

This transformation assures that identical net fluxes entering laminated poles and air gaps in the original 3D system and its slotless 2D representation cause identical MMF drops.

The transformation (9) is very simple if B(H) curve is linear. Thus for the control gap the original  $B=\mu_0 H$  dependence after transformation (9) becomes  $B=\mu_0/K_{pole0} \cdot H$ , where  $K_{pole0}$  is the pole factor on the laminated pole ID.

It can also be noticed that the main part of the laminated pole reluctance is due to the lamination insulation, which has relative permeability close to 1, rather than the laminations themselves. Because of this, B(H) curve within the lamination stack is also close to linear. To quantify how long the flux has to travel within the insulation compared to the path within the lamination material, we introduce stacking factor  $SF$ , defined as ratio of the thickness of the lamination material in a stack vs total stack thickness. Assuming that reluctance of the lamination material is negligible, it is easy to show that the effect of the winding slots can be taken into account in 2D model by redefining the stacking factor according to the following equation:

$$SF^*(r) = 1 - (1 - SF) / K_{pole}(r) \quad (10)$$

Note that the equivalent stacking factor  $SF^*$  used in the model is a function of the radius  $r$  since in general  $K_{pole}$  may vary with the radius. A practical way to reflect this dependence in the model is to split representation of the slotted portion of the laminated pole radially into several cylindrical sections with different values of  $SF^*$  as shown in Figure 5.

Finally, after the FEA is complete, one needs to do

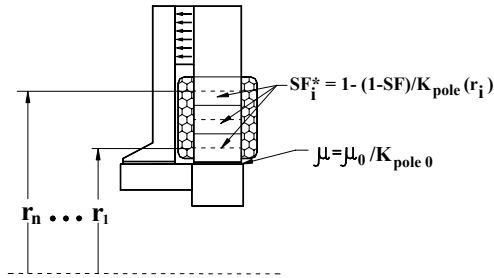


**Figure 5. Including effects of the winding slots in 2D FEA model.**

the inverse transformation to obtain bias flux density in the control air gap of the 3D system,  $B_{bias}$ . This transformation is

$$B_{bias} = B_{bias}^* / K_{pole0}, \quad (11)$$

where  $B_{bias}^*$  is the magnetic flux density calculated in the cylindrical air gap of the 2D FEA model.

Figure 6 shows flux distribution in the control air gap calculated using this technique and FEMM program (the curve is not scaled using (11)). The flux distribution is strongly non-uniform. The highest flux density occurs at the pole end closest to the magnet

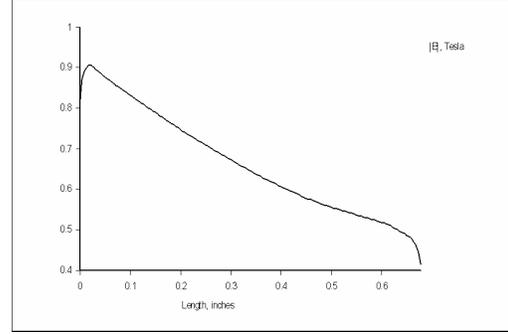


**Figure 6. Axial distribution of the bias flux density in the control air gap.**

since the flux travel shortest distance across the lamination.

#### *Negative stiffness calculation*

One of the important parameters of the magnetic bearing actuator is the destabilizing negative stiffness exerted on the rotor due to the bias flux. High negative stiffness significantly complicates control design. The negative stiffness analysis would be a three dimensional problem even if we neglected winding slots, since it implies calculation of the force exerted on the radially displaced rotor. We present an approach that allows calculation of the negative stiffness using 2D FEA. More accurately, it allows calculation of the radial force acting on the rotor displaced by some distance  $e$  from the central position.

We consider separately forces acting on the rotor due to bias magnetic fields in the air gaps of the active and passive poles  $F_A$  and  $F_P$ . The total force  $F$  can be found as a sum

$$F = F_A + F_P \quad (12)$$

#### **a. Force due to the active pole bias field**

First we consider one of the control poles. The pole length is given by the angle  $\alpha$  and its orientation with respect to the displacement is characterized by the angle  $\beta$  as shown in Figure 7. Let the nominal value of the air gap be  $g_0$ . When the rotor is displaced from the central position, the air gap becomes a function of the polar angle  $\phi$ :

$$g(\phi) = g_0 - e \cos \phi \quad (13)$$

Let  $U$  be the MMF drop between the rotor surface and the poles. When the control pole is laminated,  $U$  is nearly the same in the circumferential direction for all poles, but may vary axially, i.e.  $U$  is a function of the axial coordinate  $x$ :  $U=U(x)$ .

The magnetic field strength in the air gap is then a function of both the polar angle and the axial coordinate:

$$H(\phi, x) = \frac{U(x)}{g(\phi)} = \frac{U(x)}{g_0 - e \cos(\phi)}. \quad (14)$$

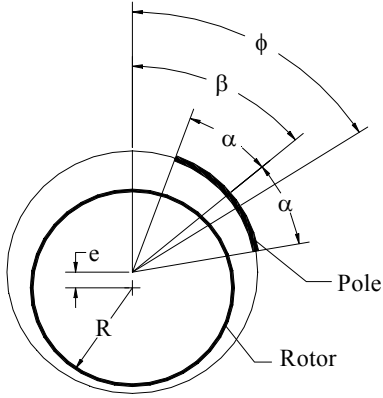


**Figure 7: Geometry for the analysis of the negative radial stiffness due to the active pole.**

The magnetic flux density in the air gap is

$$B(\phi, x) = \mu_0 H(\phi, x) = \mu_0 \frac{U(x)}{g_0 - e \cos(\phi)} \quad (15)$$

The magnetic flux through ONE pole per unit of the axial length is

$$\begin{aligned} \Phi_0(x) &= \int_{\beta-\alpha}^{\beta+\alpha} B(\phi, x) R d\phi = \\ &= \left( \mu_0 R \int_{\beta-\alpha}^{\beta+\alpha} \frac{1}{g_0 - e \cos(\phi)} d\phi \right) \cdot U(x) \end{aligned} \quad (16)$$

The integral in the brackets can be evaluated analytically. Then (16) becomes:

$$\Phi_0(x) = K_1 U(x) \quad (17)$$

where

$$\begin{aligned} K_1 &= \frac{2\mu_0 R}{\sqrt{g_0^2 - e^2}} \left\{ a \tan 2(X_1; Y_1) - \right. \\ &\quad \left. - a \tan 2(X_2; Y_2) \right\}; \\ X_1 &= \sqrt{g_0^2 - e^2} \cos\left(\frac{\beta + \alpha}{2}\right); \\ Y_1 &= (g_0 + e) \sin\left(\frac{\beta + \alpha}{2}\right); \\ X_2 &= \sqrt{g_0^2 - e^2} \cos\left(\frac{\beta - \alpha}{2}\right); \\ Y_2 &= (g_0 + e) \sin\left(\frac{\beta - \alpha}{2}\right). \end{aligned} \quad (18)$$

Note that  $\text{atan2}$  is defined in all four quadrants.

The total flux through ONE pole is

$$\Phi_1 = \int_0^L \Phi_0(x) dx = K_1 \int_0^L U(x) dx = K_1 U_{av} L_C,$$

where  $L_C$  is the axial length of the control pole and  $U_{av}$  is the average value of the MMF drop.

If we consider all four poles, the coefficients  $K_i$  will be different for each pole, but  $U(x)$  and, consequently,  $U_{av}$  will be the same.

The total flux through ALL FOUR poles will be

$$\Phi = \sum_{i=1}^4 K_{1i} \times U_{av} L_C \quad (19)$$

As a next step, we calculate force exerted by the four control poles on the rotor. The force per unit length is

$$\begin{aligned} f(x) &= \frac{1}{2\mu_0} \frac{\beta + \alpha}{\beta - \alpha} \int B(\phi, x)^2 R \cos(\phi) d\phi = \\ &= \left( \frac{\mu_0 R}{2} \frac{\beta + \alpha}{\beta - \alpha} \int \frac{\cos(\phi)}{(g_0 - e \cos(\phi))^2} d\phi \right) \times U(x)^2 \end{aligned} \quad (20)$$

Again, the integral in bracket can be evaluated analytically, yielding

$$f(x) = K_2 U(x)^2, \quad (21)$$

where

$$K_2 = \frac{\mu_0 R}{2} \left\{ \frac{\frac{g \sin(\beta + \alpha)}{(g^2 - e^2)(g - e \cos(\beta + \alpha))} - \frac{g \sin(\beta - \alpha)}{(g^2 - e^2)(g - e \cos(\beta - \alpha))}}{\frac{1}{\mu_0 R} \frac{e}{g^2 - e^2} K_1} \right\} \quad (22)$$

The total force exerted on the rotor by the FOUR control poles is

$$F_C = \left( \sum_{i=1}^4 K_{2i} \right) \int_0^L U^2(x) dx. \quad (23)$$

In the following discussion, we assume that the shape of the  $U(x)$  (and consequently the shape of  $B(x)$ ) is not affected by the rotor displacement. The magnitude of  $U(x)$ , however, is affected by the displacement.

To characterize the shape of  $U(x)$ , we introduce dimensionless  $u(x)$ :

$$u(x) = U(x)/U_{av}.$$

Note that  $U_{av}$  characterizes the magnitude (scaling factor) of  $U(x)$ . Using (19),  $U_{av}$  can be found as

$$U_{av} = \Phi / \left( L_C \sum_{i=1}^4 K_{1i} \right). \quad (24)$$

The shape function  $u(x)$  can be obtained using the field distribution in the air gap, which was calculated earlier using FEA. Indeed, using (15) we can see that  $u(x) = B(x)/B_{av}$ .

Finally we rewrite (23) using our definitions of  $U_{av}$  and  $u(x)$  as

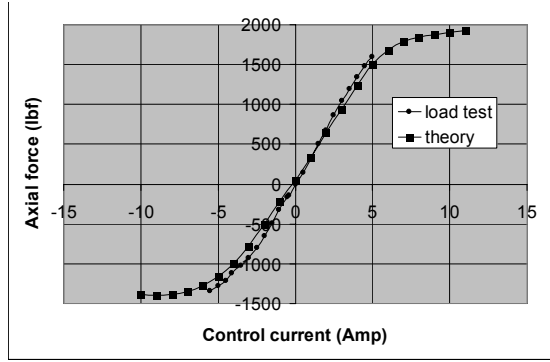


**Figure 8. Theoretical and experimental axial force vs control current curves.**

$$F_C = \frac{\sum_{i=1}^4 K_{2i}}{\left(\sum_{i=1}^4 K_{1i}\right)^2} \left(\frac{1}{L_c}\right)^2 L \int_0^L u^2(x) dx \cdot \Phi^2 \quad (26)$$

Equation (26) allows calculation of the radial force acting on the displaced rotor knowing the system geometry and direction of the displacement defined by  $L_c$  and coefficients  $K_{1i}$ ,  $K_{2i}$ ; the axial bias flux  $\Phi$  through all FOUR poles, and its axial distribution in the control gap  $u(x)$ , which can be found using 2D FEA for the central rotor position.

Regarding the total bias flux  $\Phi$ , it can be noticed that we size the cross-section of the passive pole (see Figure 3) so that it is very close to saturation. Because of this, the bias flux does not change significantly when the rotor is displaced radially.

The model can be further refined to recalculate  $\Phi$  for displaced rotor position.

#### b. Force due to the passive pole bias field

Similarly to how it was done for the active poles, it can be shown that the force exerted on the displaced rotor due to bias magnetic field in the air gap under the passive pole is

$$F_P = \frac{1}{2\mu_0} \frac{1}{2\pi RL_P} \frac{e}{\sqrt{g_0^2 - e^2}} \Phi^2, \quad (27)$$

where  $L_P$  is the axial length of the passive pole. It can be learned from (27) that radial force  $F_P$ , and correspondingly the negative stiffness, can be reduced by increasing the passive pole surface area  $2\pi RL_P$ . In our design it is realized through extending the pole axially as shown in Figure 3. The extended pole foot fits under end turns of the neighboring generator.

### BEARING TEST RESULTS

The above described Gas Expander/Generator has been built and tested. The measured characteristics of

the magnetic bearings are in very close agreement with predictions. Figure 8 shows experimental and theoretical force vs current curves obtained with the above described asymmetric thrust bearing. The theoretical curve was calculated using FEMM program.

It can be observed that the bearing does have different load capacities in different directions while the force vs current dependence remains linear until the actuator start saturating.

We have also measured force vs current curve and negative stiffness of the radial bearings. When calculating negative stiffness force using equations (12), (26) and (27) for comparison with the experimental value, we used a value of the bias flux  $\Phi$  adjusted to produce experimentally measured radial force vs control current gain. With this correction, the discrepancy between the theoretical and measured values of the negative stiffness was less than 5%.

### CONCLUSION

The magnetic bearing system that we have developed, built and tested for application in the new generation gas expanders features several novel technical solutions including anisotropic axial bearing and homopolar PM-biased high-efficiency radial magnetic bearings. The axial magnetic bearing has different pole areas on the opposite sides of the thrust disk, which simplifies its integration into the system. Regardless this fact, it offers linear force vs control current dependence, which significantly simplifies the control algorithm.

Using PM bias in the radial bearings results in a very compact and highly efficient design, which very advantageous feature is that the control flux does not flow through high reluctance permanent magnets. This minimizes size of the control coils as well as their power dissipation.

We have developed analysis methods which allow accurate calculation of the bias flux density and negative stiffness for this type of bearing using 2D FEA, in spite of the three-dimensional nature of the problem. The analysis results are found in good agreement with experimental data.

### REFERENCES

1. Meeks, C.R., DiRusso, E., Brown, G.V., 1990, "Development of a Compact, Light Weight Magnetic Bearing", AIAA/SAE/ASME/ASEE 26th Joint Propulsion Conference, Orlando.
2. <http://femm.foster-miller.com/>